molecular pharmaceutics

Article

pubs.acs.org/molecularpharmaceutics

A Novel Lanreotide-Encoded Micelle System Targets Paclitaxel to the Tumors with Overexpression of Somatostatin Receptors

Nan Zheng,[†] Wenbing Dai,[†] Wenwen Du,[†] Haoran Zhang,[†] Liandi Lei,[†] Hua Zhang,[†] Xueqing Wang,[†] Jiancheng Wang,[†] Xuan Zhang,[†] Jinming Gao,[‡] and Qiang Zhang*[,†]

[†]State Key Laboratory of Natural and Biomimetic Drugs, School of Pharmaceutical Sciences, Peking University, Beijing, People's Republic of China

[‡]Harold C. Simmons Comprehensive Cancer Center, Department of Pharmacology, UT Southwestern Medical Center, Dallas, Texas 75390, United States

Supporting Information

ABSTRACT: Many tumor cells specifically overexpress somatostatin receptors, in particular, subtype 2 (SSTR2). Lanreotide, a somatostatin analogue with high affinity for SSTR2, can be exploited as a ligand for tumor targeted therapy. In this study, lanreotide was first conjugated to poly(ethylene glycol)-*b*-poly(ε-caprolactone) (PEG-b-PCL) copolymer, and the active targeting micelles with paclitaxel (lanreotide-PM-PTX) or fluorescent agent were constructed and characterized with various analytical methods. Lanreotide-PM-PTX micelles were spherical in shape with a hydrodynamic diameter of 43.2 ± 0.4 nm, high drug encapsulation (87.1 ± 2.8%) and slow drug release rate. Two cancer cell lines (human lung cancer H446 and human breast cancer MCF-7 cells) with different expression levels of SSTR2 were used in this study. As observed by flow cytometry, confocal microscopy and cytotoxicity studies, lanreotide-encoded PEG-b-PCL micelles demonstrated more specific cell uptake and cytotoxicity in SSTR2-positive tumor cells via a receptor-mediated mechanism over the passive targeting micelles. The active targeting micelles showed higher accumulation in tumor tissue and tumor cells in tumor-bearing mice *in vivo* by near-infrared fluorescence (NIRF) imaging, high-performance liquid chromatography and confocal microscopy, respectively. Furthermore, treatment with lanreotide-PM-PTX micelles resulted in stronger tumor inhibition, increased life span and enhanced tumor cell apoptosis in SSTR2-overexpressing tumor model in athymic nude mice. The *in vivo* efficacy test with both H446 and MCF-7 tumor models further demonstrated the involvement of receptor-mediated interaction. Finally, the active targeting micelles exhibited less body weight loss, lower hemolysis and lower myelosuppression, as compared with the control groups. In conclusion, lanreotide can serve as an effective homing peptide, and the lanreotide-modified PEG-b-PCL micelles hold considerable promise in the treatment of SSTR2-overexpressing solid tumors.

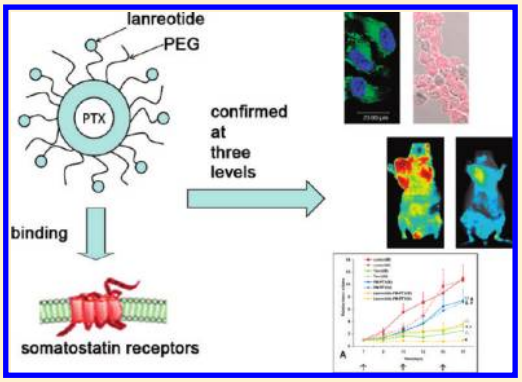

KEYWORDS: *lanreotide, somatostatin receptors, paclitaxel, active targeting micelles, receptor-mediated cellular uptake, distribution in tumor, antitumor efficacy, toxicity*

1. INTRODUCTION

Polymeric micelles (PM) are core−shell nanoparticles (5−100 nm in diameter) that are self-assembled from amphiphilic blocks or graft copolymers in aqueous media. The hydrophobic core of micelles renders effective loading of hydrophobic antitumor drugs, and the hydrophilic corona shells provide particle stabilization in aqueous solution and prevent rapid uptake by the reticuloendothelial system (RES).[1−3] Consequently, the micelle system provides several therapeutic advantages including decreased drug side effects and increased antitumor efficacy due to the enhanced permeability and retention (EPR) effect and long blood circulation.[4−6] Currently, there are several micelle systems incorporated with anticancer agents under clinical evaluation,[7] including NK105 (paclitaxel-loaded polyethylene glycol-(L-aspartic acid) micelles),[8] NK012 (SN-38, ethylhydroxycamptothecin-conjugated polyethylene glycol-poly(L-glutamic acid) micelles),[9] NC-6004 (cisplatin-loaded polyethylene glycol-poly(L-benzylglutamic acid) micelles),[10] and SP1049C (doxorubicin-loaded Pluronic micelles).[11] Furthermore, Genexol-PM, the paclitaxel incorporated PEG-PLA micelle system, has been approved in South Korea for cancer treatment .[12]

Despite many advantages, a significant challenge for micelle delivery systems is how to increase the selectivity to tumor cells and enhance targeting efficiency at the tumor sites.[13] One

Received: September 11, 2011
Revised: February 4, 2012
Accepted: March 21, 2012
Published: March 21, 2012

strategy to achieve cancer-targeted drug delivery is the modification on micelle system with targeting ligands, such as folate,[14] arginine−glycine−aspartic acid tripeptide (RGD),[15] luteinizing hormone-releasing hormone (LHRH),[16] and epidermal growth factor (EGF),[17] which could recognize the unique molecular markers overexpressing in the different cancer cells.

Somatostatin receptors (SSTRs), with five subtypes (termed as SSTR1−5), are found to be overexpressed in a variety of cancers, including human neuroendocrine tumors, pituitary adenomas, endocrine pancreatic tumors, paragangliomas, pheochromocytomas, small cell carcinomas, medullary thyroid carcinomas and adenocarcinomas of the breast, ovary and colon.[18,19] Somatostatin and its analogues can specifically bind with SSTRs. High expressions of SSTR in tumors indicate that it is a good target for tumor diagnosis and treatment. More specifically, ^{111}In-DTPA-octreotide was approved by the FDA in June 1994 for the diagnosis of various neuroendocrine tumors.[20] Other studies include the conjugation of somatostatin or its analogues to radioactive isotopes or cytotoxic drugs,[21] such as ^{125}I conjugated Tyr^3-octreotide,[22] ^{90}Y conjugated Tyr^3-octreotide,[23] octreotide conjugated paclitaxel,[24] and camptothecin−somatostatin conjugates.[25]

Lanreotide is an octapeptide analogue of endogenous somatostatin and has a high affinity for SSTR2.[26] Previous studies have demonstrated the usefulness of ^{111}In labeled lanreotide[27] and ^{177}Lu-DOTA-lanreotide[28] in the diagnostic imaging of a wide variety of tumors through the efficient targeting of lanreotide to neuroendocrine tumors and lymphomas. Compared to octreotide (a somatostatin analogue), lanreotide exhibits higher affinity for SSTR2, -3, -4 and -5, especially a modest 2-fold increase for SSTR2.[29] Besides, lanreotide as a ligand is more stable *in vivo*.[30] However, few studies have assessed lanreotide as a homing ligand in antitumor drug delivery systems. Therefore, the motivation of this work is to investigate the lanreotide-mediated drug delivery system (DDS) for the treatment of SSTR2-overexpressing tumors *in vitro* and *in vivo*.

Paclitaxel (PTX), a potent anticancer drug, has been used with success in patients with various tumors after it was approved by the FDA in 1992. In clinic, the current formulation for paclitaxel is made with Cremophor EL and ethanol (1:1, v/v). Unfortunately, this formulation results in serious side effects, such as hypersensitivity, nephrotoxicity and neurotoxicity.[31] Consequently, there is a strong impetus to improve the delivery of PTX using a safer vehicle. The block copolymer poly(ethylene glycol)-*b*-poly(ε-caprolactone) (PEG-b-PCL) has been well studied in the field of drug delivery systems due to its biodegradability and biocompatibility,[32] and was successfully used to improve the solubility of paclitaxel.[33]

To prove the hypothesis that lanreotide may achieve SSTR2-targeted tumor cell-/tissue-specific drug delivery, here we developed PTX encapsulated and lanreotide-encoded PEG-b-PCL micelles (lanreotide-PM-PTX) with PTX-loaded PM (PM-PTX) prepared as the control. As shown in our previous work, human small cell lung cancer H446 and human breast cancer MCF-7 cells had high and low expression levels of SSTR2, respectively,[34] and they were chosen as cell models. The targeting effect of lanreotide-modified micelles was investigated by their specificity to tumor cells *in vitro*, preferential accumulation in tumor tissue and cancer cells, as well as their antitumor efficacy in BALB/c mice bearing H446 or MCF-7 xenograft.

2. MATERIALS AND METHODS

2.1. Materials. Lanreotide (M_w = 1096.3 Da) was custom synthesized (purity 95%) by GL Biochem Ltd. (Shanghai, China). *N*-Hydroxysuccinimidyl-PEG$_{4000}$-b-PCL$_{2500}$ (NHS-PEG-b-PCL, M_w/M_n = 1.26) and mPEG$_{3000}$-b-PCL$_{2500}$ (M_w/M_n = 1.09) were purchased from Advanced Polymer Materials Inc. (Montreal, QC, Canada). Paclitaxel was obtained from Haikou Pharmaceutical Co., Ltd. (Hainan, China). Taxol was commercially available from the local hospital of Beijing (Bristol-Myers Squibb Co., Princeton, NJ, USA), containing 30 mg of paclitaxel in a 5 mL mixture of Cremophor EL and ethanol (1:1, v/v). DiD was provided by Biotium, Inc. (Hayward, USA). Hoechst 33258 was purchased from Molecular Probes Inc. (USA). Sulforhodamine B (SRB), 6-coumarin (C6, purity >99%), and Tris-base were from Sigma-Aldrich (St. Louis, MO, USA). In situ cell death detection kit and TMR red were the products of Roche Diagnostics GmbH (Mannheim, Germany). Cell culture media RPMI-1640, penicillin−streptomycin and trypsin were from M&C Gene Technology (Beijing, China). Fetal bovine serum was purchased from GIBCO, Invitrogen Corp. (Carlsbad, CA, USA). All other solvents and reagents were of analytical grade and used as received.

H446 and MCF-7 cells were obtained from the Institute of Basic Medical Science (Beijing, China). Cells were cultured in RPMI-1640 medium supplemented with 10% fetal bovine serum, 100 U/mL penicillin and 100 μg/mL streptomycin at 37 °C in 5% CO_2 atmosphere.

Male Sprague−Dawley rats (180−200 g) and female BALB/c nude mice (18−20 g) were purchased from Vital Laboratory Animal Center (Beijing, China) and acclimated at 25 °C and 55% of humidity under natural light/dark conditions for 1 week before the study, with free access to standard food and water (Vital Laboratory Animal Center, Beijing, China). All care and handling of animals were performed with the approval of Institutional Animal Care and Use Committee at Peking University Health Science Center.

2.2. Synthesis of Lanreotide−PEG-b-PCL Copolymer. Lanreotide was conjugated to PEG-b-PCL through the NHS group. Briefly, NHS-PEG-b-PCL was dissolved in DMSO with lanreotide at a 1.5:1 molar ratio, adjusting pH to 8−9 with triethylamine. The reaction proceeded for 2 days at room temperature under moderate stirring and monitored by reversed phase high-performance liquid chromatography (RP-HPLC, Shimadzu, LC-10AT, Japan) at 220 nm. The mobile phase was a mixture of acetonitrile and water (28:72, v/v) containing 0.1% trifluoroacetic acid. Then the reaction mixture was dialyzed (molecular mass cutoff 3500 Da) against deionized water for 48 h to remove unconjugated peptide. The final solution was lyophilized and stored at −20 °C until use. The formation of lanreotide−PEG-b-PCL copolymer was confirmed by the nuclear magnetic resonance spectra (^{1}H NMR, Bruker Avance-III 400 MHz, Bruker BioSpin, Swiss).

2.3. Preparation of PTX-Loaded PM. The lanreotide-modified PEG-b-PCL micelles containing paclitaxel (lanreotide-PM-PTX) were prepared by a thin-film hydration method, as described previously.[35] Briefly, PTX, mPEG-b-PCL and lanreotide−PEG-b-PCL (1:20:5, w/w/w) were codissolved in acetonitrile, and the solvent was evaporated at 60 °C until dry. The obtained copolymer film was hydrated in 5% glucose solution at 60 °C, and the system was sonicated for 2 min until a clear micelle solution was obtained. Finally, the solution was

filtered through a 0.22 μm membrane. The final concentration of PTX and polymer is 2 mg/mL and 50 mg/mL, respectively. For the preparation of PM-PTX, an identical procedure was conducted except that the equivalent amount of lanreotide−PEG-b-PCL was replaced by mPEG-b-PCL. By the way, we did not separate free polymer from micelles since the critical micelle concentration of mPEG-b-PCL was low (3.69 μg/mL).[36] Compared to the final concentration of polymer, the concentration of free polymer is so low that it would bring very limited effect. Moreover, separation will break the balance between the free polymer and the micelles, and accordingly form free polymer again.

2.4. Characterization of PTX-Loaded PM. The particle size and surface charge of PTX-loaded PM were determined by dynamic light scattering (DLS) using a Malvern Zetasizer Nano ZS (Malvern, U.K.) at 25 °C. The encapsulation efficiency of PTX in micelles was quantified by a HPLC system. Micelle solution was eluted in a C18 column with a mobile phase containing methanol, acetonitrile and water (40:30:30, v/v/v) at a flow rate of 1.0 mL/min, and detected at 227 nm. The shape and surface morphology of lanreotide-PM-PTX were investigated by transmission electron microscope (TEM, JEOL, JEM-1400, Japan) after negative staining with 1% phosphotungstic acid solution.

The release of PTX from micelles was studied using the dialysis method. Briefly, 0.25 mL of micelles was mixed with 0.75 mL of release medium (1 M sodium salicylate)[37] and placed in a dialysis bag (molecular mass cutoff 14,000 Da). The mixture was dialyzed against 80 mL of release medium at 37 °C with stirring at 100 rpm. Aliquots of release medium were sampled at designated time points (0.5, 1, 3, 5, 7, 12, 24, 48 h) and replaced with an equal volume of fresh medium. Released PTX was quantified using the HPLC method described above.

X-ray diffraction (XRD) measurements of PTX powder, lyophilized blank micelles and lyophilized PTX-loaded micelles were carried out on an X-ray diffractometer (Dmax 2400, Rigaku Corporation, Japan) with Cu Kα radiation (λ = 1.5406 Å) at room temperature. The scanning speed was 4°/min, and the XRD patterns were recorded by scanning 2θ angles from 3° to 50° in a scan mode (0.02°) at 40 kV and 100 mA. The slit widths were set at 1/2° for DS, 1/2° for SS and 0.3 mm for RS.

Fourier transform infrared (FTIR) spectra were recorded on a Fourier transform infrared spectrometer (NEXUS-470, Thermo Nicolet Corporation, USA) over the range of 4000—500 cm^{-1} by accumulating 32 scans at a resolution of 8 cm^{-1} with sample gain of 8.0, mirror velocity of 0.6329 and aperture of 100.00. In each experiment, PTX powder, lyophilized blank micelles and lyophilized PTX-loaded micelles were mixed with potassium bromide at a ratio of 1:99 (w/w) to make into disks before measurements.

2.5. Preparation and Characterization of C6 or DiD-Loaded PM. The preparation of C6- or DiD-loaded PM (PM-C6, PM-DiD, lanreotide-PM-C6 and lanreotide-PM-DiD) was the same as that of PTX-loaded PM, except that PTX was replaced by C6 or DiD. The final concentration of C6 and polymer is 10 μg/mL and 10 mg/mL, respectively; and the final concentration of DiD and polymer is 10 μg/mL and 20 mg/mL, respectively. Besides the DLS measurement as mentioned above, the encapsulation efficiency of C6 or DiD was evaluated via fluorescence spectroscopy (C6, λ_{ex} 458 nm, λ_{em} 497 nm; DiD, λ_{ex} 648 nm, λ_{em} 662 nm) using a fluorescence spectroscope (Cary Eclipse, Varian Corporation, USA), after dilution with DMSO.

To study the release kinetics of C6 loaded micelles, 1 mL micellar solutions were mixed with 1 mL of RPMI-1640 containing 10% FBS. Then the diluted solutions were transferred to the dialysis bag (molecular weight cutoff 14,000 Da) and dialyzed against 100 mL of RPMI-1640 containing 10% FBS under continuous gentle stirring at 37 °C. Released C6 was quantified using fluorescence spectroscopy described above.

2.6. Flow Cytometry Studies. C6 was used as a hydrophobic fluorescent probe to study cellular uptake of PM.[38] Approximately 7 × 10^5 H446 cells or 5 × 10^5 MCF-7 cells per well were seeded in a 6-well plate 24 h prior to study, and cells were incubated at 37 °C for 1 h, 3 and 6 h with C6-loaded PM (100 ng/mL of C6). Then, cells were trypsinized, pelleted by centrifugation, washed three times with cold PBS and finally examined by a flow cytometer (FACScan, Becton Dickinson, San Jose, CA), excited at 488 nm and detected at 560 nm. Data were analyzed with the FACStation software.

In the receptor competitive experiment, excess of free lanreotide (2.5 mg/mL) was added to the serum-free culture medium and incubated at 37 °C for 0.5 h prior to the addition of lanreotide-PM-C6. Then cells were incubated at 37 °C for 6 h with each micelle solution, and detected with the same procedures mentioned above.

2.7. Confocal Microscopy Studies. Following 24 h incubation of H446 cells or MCF-7 cells on glass bottom dishes containing growth media at 37 °C, active targeting or passive targeting PM-C6 micelles (100 ng/mL) were added to each dish and were incubated at 37 °C for another 6 h. In competition experiments, an excess of free lanreotide (2.5 mg/mL) was added to the culture medium 30 min prior to the addition of C6-loaded PM. The medium was removed and cells were washed with cold PBS followed by fixing with 4% paraformaldehyde in PBS. Then cells were treated with Hoechst 33258 (λ_{ex} 352 nm, λ_{em} 460 nm) for 5 min, and the fluorescent images of cells were analyzed using a laser scanning confocal microscope (LSCM, Leica, TCS SP5, Germany).

2.8. *In Vitro* Cytotoxicity Studies. The cytotoxicity of PTX formulations against H446 cells was assessed by the SRB assay as originally described.[39] In brief, cells in exponential growth were seeded at a density of 5000 cells/well in 96-well plates. After 24 h, cells were exposed to various concentrations of PTX in different formulations. Another 48 h incubation was conducted before the cells were fixed with trichloroacetic acid, washed and stained with SRB. Absorbance was recorded at 540 nm using a 96-well plate reader (Biorad, 680, America), and the drug concentration which inhibited the cell growth by 50% (IC_{50}) was determined from semilogarithmic dose−response plots.

2.9. *In Vivo* Distribution Studies by Living Imaging Studies and HPLC Analysis. DiD, a near-infrared carbocyanine dye, has low toxicity, does not require histochemical processing prior to visualization, and is highly lipophilic, so that it has been successfully used in tracing cortical fibers, neurons and cellular uptake.[40−42] As it allows the noninvasive visualization of *in vivo* activity of the rerouted nanoparticles in living animals, here we employed DiD as a near-infrared fluorophore encapsulated in the micelles to evaluate the biodistribution of DiD-loaded PM in H446 tumor-bearing nude mice.

When tumor size reached 300 mm^3, mice were injected with 0.2 mL of 5% glucose, free DiD, PM-DiD or lanreotide-PM-DiD (100 μg/kg DiD) via the tail vein, respectively, and then

anesthetized by 2% isoflurane delivered via a nose cone system. NIRF imaging experiments using a Maestro *in vivo* imaging system (CRI, Woburn, MA, USA; excitation = 575−605 nm, emission = 645 nm long pass) were performed at 0.17, 1, 3, 5, 10, and 24 h postinjection. After living imaging, mice were sacrificed. Tumors and organs were excised and analyzed again with the same system. The images were analyzed with the imaging station Maestro software.

To quantify the drug accumulation in tumor with time accurately, drug distribution in mice bearing H446 tumor was evaluated by HPLC. After tumor volume reached approximately 300 mm^3, PM-PTX and lanreotide-PM-PTX were intravenously administered via lateral tail veins at a dose of 400 μg/mouse. At scheduled time points (0.17, 0.33, 0.67, 1, 2, 5, 10, 24 h) after injection, the tumors were excised, weighed and homogenized in phosphate buffered saline (1:1 w/v). After adding 100 μL of norethisterone (2.5 μg/mL in acetonitrile) as an internal standard, the samples were extracted with methyl *tert*-butyl ether. After vortexing for 5 min and centrifuging for 10 min at 4000 rpm, the supernatant was removed and dried in nitrogen gas. The dried residues were reconstituted in mobile phase and injected onto a HPLC system with an UV detector at 227 nm. The sample was eluted with a mobile phase consisting of acetonitrile and water (50:50, v/v) at a flow rate of 1.0 mL/min.

2.10. *In Vivo* Cellular Uptake Studies. To further study the *in vivo* cellular uptake after NIRF imaging experiments, the harvested H446 tumors from living imaging studies were immediately frozen in OCT medium (Sakura Finetek), cut into 5 μm thick sections using a microtome, and viewed in the confocal microscope by bright-field illumination and fluorescence. Besides, the frozen section was stained with hematoxylin and eosin (H&E), and observed under an optical microscope to confirm its tissue morphology.

2.11. *In Vivo* Antitumor Activity. *Antitumor Efficacy.* The antitumor efficacy was investigated in H446 or MCF-7 tumor-bearing mouse models. Briefly, 2.5×10^6 H446 cells were injected subcutaneously in the armpits of nude mice. On the seventh day, H446 tumor-bearing mice were randomly assigned to one of the following four groups ($n = 6$): group 1 for 5% glucose solution, group 2 for Taxol injection (20 mg/kg), group 3 for PM-PTX (20 mg/kg), and group 4 for lanreotide-PM-PTX (20 mg/kg). Mice were administered through the tail vein every 4 days for 3 times. Throughout the study, tumor volume of each mouse was monitored every two days with a caliper, and calculated by the following formula: $V = (\text{major axis}) \times (\text{minor axis})^2 \times 1/2$. After the final administration, the mice were further observed for another 2 days before they were sacrificed on the 17th day. Two sections were made from each tumor stripped from test mice, which was used for H&E staining and TUNEL analysis, respectively. MCF-7 tumor-bearing mice were operated as above except that 1.3×10^6 MCF-7 cells were subcutaneously injected in the armpits of nude mice.

H&E Analysis. The samples obtained from the harvested H446 tumors of the antitumor efficacy study were fixed in 10% formalin and embedded in paraffin, and then 5 μm sections were prepared. They were placed on glass slides, deparaffinized in xylen, and dehydrated in graded alcohols. These slides were stained with hematoxylin and eosin (H&E), and finally observed under an optical microscope.

Survival Study. In the study of animal survival, the H446 tumor-bearing mouse model and the dose regimen were the same as above, except that a total of 40 mice were randomized into four groups (10 mice/group). Mice were checked for survival every day for 40 days.

2.12. TUNEL Assay. Apoptosis of tumor cells was detected by terminal deoxynucleotide transferase (TdT)-mediated dUTP nick-end labeling (TUNEL) assay. It was performed using In Situ Cell Death Detection Kit (TMR red, Roche, Mannheim, Germany) as per the manufacturer's protocol. Briefly, the samples obtained from the harvested H446 tumors of antitumor efficacy study were frozen in OCT embedding medium, cut into 5 μm thick sections, and fixed in 4% (v/v) paraformaldehyde for 10 min at room temperature. They were washed with PBS twice and incubated with 0.1% (v/v) Triton X-100 for 2 min on ice. After the samples were washed twice with PBS, TUNEL reaction mixture containing equilibration buffer, nucleotide mix and TdT enzyme was added to the tissue sections, which were then incubated in a dark humid atmosphere at 37 °C for 1 h. The samples were washed three times with PBS to remove unincorporated fluorescein-dUTP. Then the samples were treated with Hoechst 33258 for 30 min and then analyzed using a laser scanning confocal microscope (LSCM, Leica, TCS SP5, Germany).

2.13. Toxicity Study. *Blood Analysis and Body Weight Change.* H446 cells were injected subcutaneously at 2.5×10^6 density in the armpits of nude mice. When the tumor volume reached about 150 mm^3 on the seventh day, mice were randomly assigned to one of the following five groups ($n = 6$): group 1 for 5% glucose solution, group 2 for Taxol injection (20 mg/kg), group 3 for the corresponding Taxol vehicle (50% Cremophor EL and 50% ethanol), group 4 for PM-PTX (20 mg/kg), and group 5 for lanreotide-PM-PTX (20 mg/kg). Mice were administered through the tail vein at days 7, 11, and 15 after inoculation. The body weight of each mouse was monitored every two days. On day 22, heparinized retro-orbital sinus blood samples were collected, and hemoglobin (HGB) and white blood cells (WBC) were counted with a hemocytometer.

Hemolysis Test. Blood was freshly drawn from a male Sprague−Dawley rat by cardiac puncture. The blood was washed with 0.1 M phosphate-buffered saline (PBS, pH 7.4) and centrifuged at 600*g* for 5 min. Its supernatant was pipetted off repeatedly. The red blood cell (RBC) suspension was diluted with PBS to 2% (w/v). RBC suspension (2 mL) was added to a 2 mL test sample with a concentration from 0.01 to 1 mg/mL. After incubation at 37 °C for 1 h, the mixture was centrifuged at 3000 rpm for 10 min to remove nonlysed RBC. The supernatant was collected and analyzed by spectrophotometric determination at 576 nm ($n = 3$). To obtain 0 and 100% hemolysis, 2 mL of RBC suspension was added to 2 mL of PBS and 2 mL of distilled water, respectively. The degree of hemolysis was calculated by the following equation: hemolysis (%) = (Abs − Abs0)/(Abs100 − Abs0) × 100, where Abs, Abs100 and Abs0 are the absorbance of the test sample, distilled water and PBS, respectively.[43]

2.14. Statistical Analysis. All the experiments were repeated at least three times. All data are shown as means ± standard deviation (SD) unless particularly outlined. Student's *t* test or one-way analyses of variance (ANOVA) were performed in statistical evaluation. A *p*-value less than 0.05 was considered to be significant, and a *p*-value less than 0.01 was considered as highly significant.

Table 1. Characteristics of PEG-b-PCL Polymeric Micelles (n = 3)

preparations	particle size (nm)	polydispersity (PDI)	zeta potential (mV)	encapsulation efficiency (%)	loading efficiency (mol %)
blank PM	32.8 ± 1.3	0.17 ± 0.05	−2.78 ± 1.73		
PM-PTX	38.3 ± 0.1	0.18 ± 0.03	−3.87 ± 2.89	90.0 ± 2.9	20.2
lanreotide-PM-PTX	43.2 ± 0.4	0.15 ± 0.05	−4.82 ± 2.31	87.1 ± 2.8	20.7
PM-C6[a]	34.6 ± 0.7	0.16 ± 0.06	−4.44 ± 0.34	96.5 ± 3.7	1.63
lanreotide-PM-C6[a]	47.6 ± 1.0	0.18 ± 0.01	−4.97 ± 1.85	83.1 ± 6.0	1.49
PM-DiD	45.9 ± 0.9	0.24 ± 0.09	−4.65 ± 0.78	86.8 ± 3.2	0.25
lanreotide-PM-DiD	53.1 ± 1.2	0.19 ± 0.09	−5.20 ± 1.56	82.1 ± 4.8	0.25

[a]C6 represents 6-coumarin.

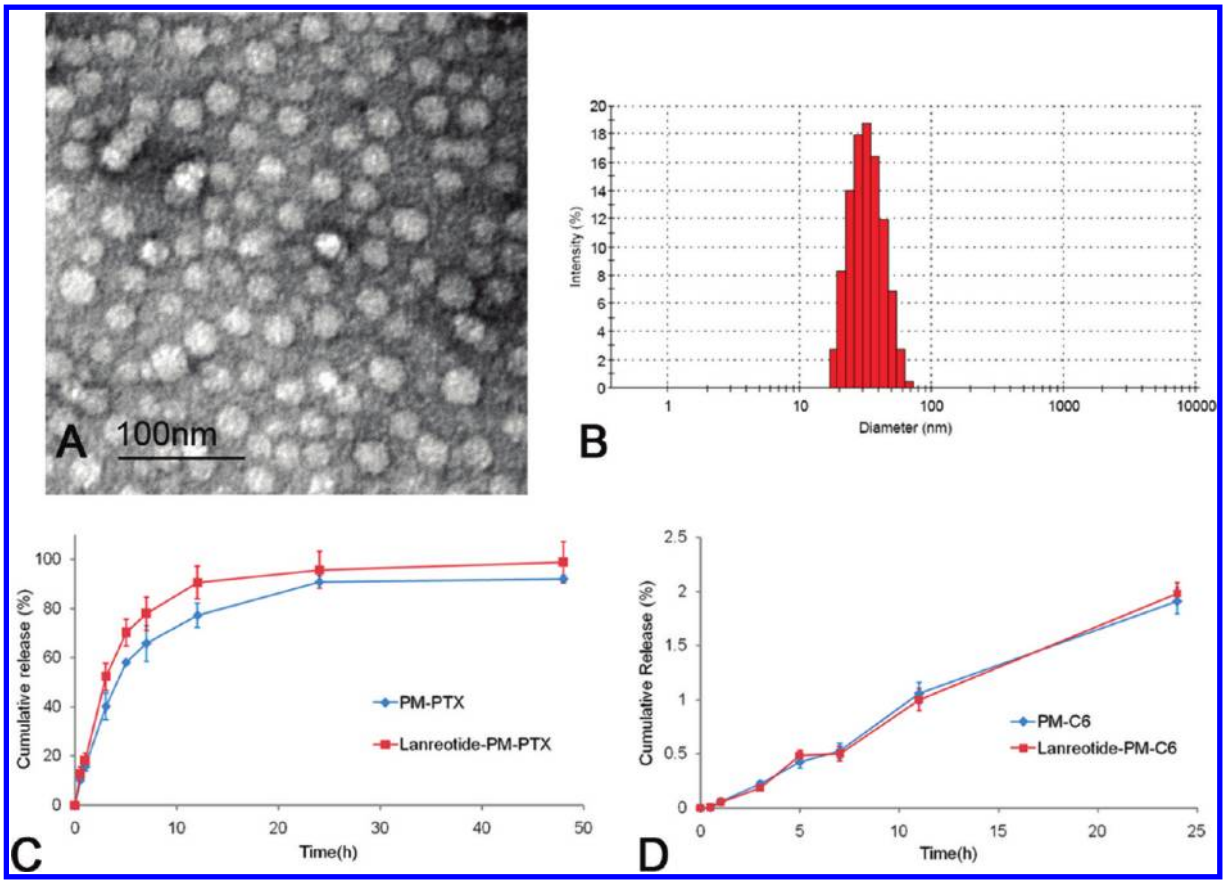

Figure 1. (A) A typical TEM image of PTX-loaded lanreotide-conjugated PEG-b-PCL micelles stained with 1% phosphotungstic acid. Scale bar is 100 nm. (B) A representative particle size distribution profile of lanreotide-PM-PTX by dynamic light scattering. (C) *In vitro* release of PTX from micelles. 0.25 mL of PTX-loaded micelles were mixed with 0.75 mL of release medium (1 M sodium salicylate) and placed in a dialysis bag (molecular mass cutoff 14,000). The mixture was dialyzed against 80 mL of release medium at 37 °C under the stirring of 100 rpm. Each point represents the mean ± SD of three samples. (D) *In vitro* release of C6 from micelles in RPMI-1640 containing 10% FBS at 37 °C.

3. RESULTS AND DISCUSSION

3.1. Synthesis of Lanreotide−PEG-b-PCL. Lanreotide was conjugated to the NHS-PEG-b-PCL copolymer through a reaction between the NHS group and the N-terminal amino group of the cyclic peptide. The conjugation reaction was monitored by RP-HPLC and the final product was characterized by ^{1}H NMR (see Figure S1 in the Supporting Information). The conjugation efficiency reached to 81.9 ± 3.5% after reacting for 48 h at room temperature. The ^{1}H NMR of reaction product showed a multiplet at δ 7.1−7.9 ppm from phenyl protons, which is characteristic of lanreotide. These results suggested that lanreotide could be successfully conjugated to NHS-PEG-b-PCL via an amide bond.

3.2. Preparation and Characterization of Various Micelle Systems. PTX is extremely hydrophobic, and it has a low water solubility at 0.3 μg/mL.[44] However, previous work showed that PEG-b-PCL micelles could solubilize PTX to about 2 mg/mL in aqueous solution, approximately 4 orders of magnitude increase over its solubility in water.[45]

The prepared PEG-b-PCL polymeric micelles with or without lanreotide and their properties are listed in Table 1. The mean particle size for all formulations was between 30 and 55 nm with a polydispersity (PDI) less than 0.25. The modification of lanreotide in the modified polymer micelle was 7.66% (mol %). The peptide modification increased the particle size, and the particle size difference between micelles loaded with PTX and fluorescent agent was less than 10 nm. It is well documented that the receptor-mediated endocytosis is the most important pathway in intracellular delivery for all the nanoparticles less than 150 nm,[46,47] so the prepared dye-

dx.doi.org/10.1021/mp200464x | *Mol. Pharmaceutics* 2012, 9, 1175−1188

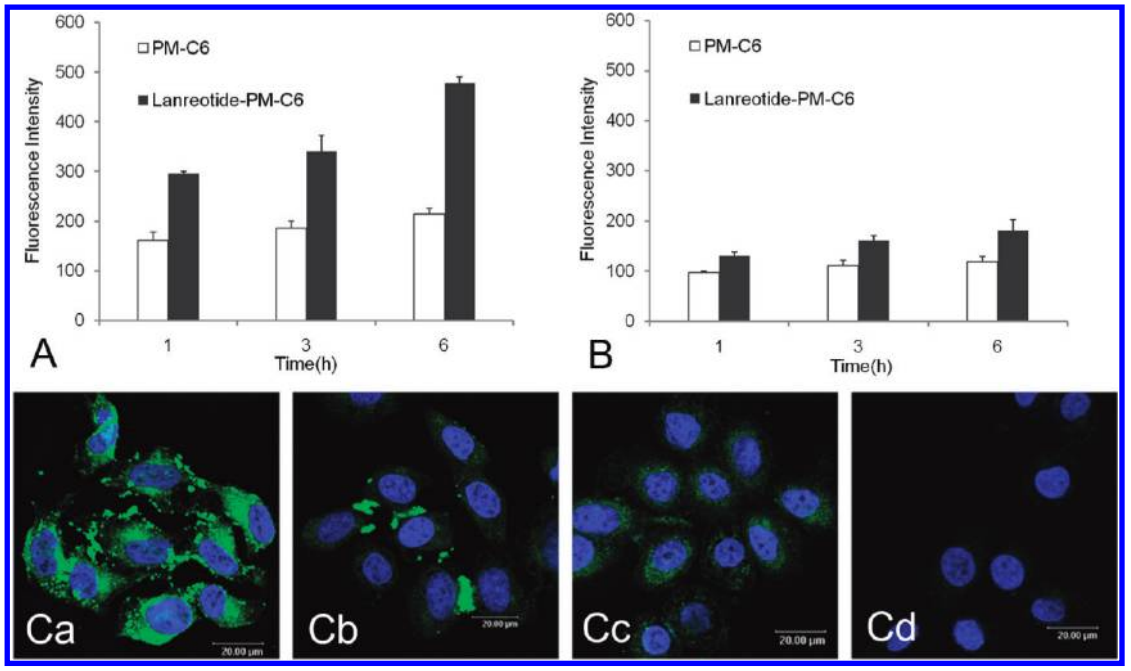

Figure 2. The uptake of PM-C6 and lanreotide-PM-C6 by (A) H446 cells and (B) MCF-7 cells at 37 °C at different times, monitored by flow cytometry. Each point represents mean fluorescence intensity ± SD (n = 3). Confocal microscopy images (C) of H446 (a, b) and MCF-7(c, d) after incubation with lanreotide-PM-C6 (a, c) and PM-C6 (b, d) at 37 °C for 6 h. The concentration of C6 was 100 ng/mL for all formulations. Green represents fluorescence of C6. Blue represents fluorescence of Hoechst 33258.

labeled micelles can be used to trace the fate of drug-loaded micelles at the cellular level or the animal level in this study. On the other hand, the encapsulation efficiency for PTX was higher than 82% and all micelle systems exhibited a weak negative surface charge of less than −5.50 mV. The slight anionic charge on the micellar surface might avoid the nonspecific organ uptake, and then offer a better targeting effect *in vivo*.[48]

Characteristics of lanreotide-PM-PTX are presented in Figure 1. The active targeting micelles were about 30−40 nm and had a narrow particle size distribution, with uniform spherical structure (Figure 1A,B). As seen in Figure 1C, there were no significant differences in drug release at each time point between micelles with or without lanreotide, indicating little effect from the peptide modification. Actually, the drug release was rather slow, considering a solubilizer (sodium salicylate) added in the release medium. Additionally, the C6 released comparably from both micellar systems in a medium similar to the cell culture (Figure 1D). More than 98% of the fluorescent probe was still remaining in micelles after 24 h. Therefore, most C6 may remain in the micellar carrier during the cellular experiment. The final concentration of C6 in the release medium at 24 h was less than 0.002 μg/mL, which was much lower than its saturation solubility (0.049 ± 0.006 μg/mL),[49] and a perfect sink condition could be confirmed. On the other hand, previous work showed that lipophilic carbocyanine fluorescent dye (e.g., DiD) released from nanoparticles very slowly and could be used to investigate the *in vivo* distribution activity of micelles.[50,51] Moreover, when stored at 4 °C, no significant leakage of PTX from micelles was found within one week.

The XRD curves of different formulations are shown in Figure S2A in the Supporting Information. The blank micelles were amorphous, so they showed relatively wide and broad peaks in its XRD curve, while the PTX crystals exhibited many distinct sharp peaks which disappeared in the PTX-loaded micelles, indicating that PTX exists in the inner core of micelles in a molecular or amorphous dispersion.

As presented in the FTIR spectra (see Figure S2B in the Supporting Information), PTX showed the characteristic bands at 3512, 3440, 3406 (ν_{NH}) and 1647 ($\nu_{C=O}$) cm^{-1}, as well as the bands of benzene ring at 1450, 1500, and 1600 cm^{-1}. After encapsulation of PTX in micelles, there was no new peak appearing in PM-PTX and the positions of PTX peaks did not change significantly, revealing that PTX is physically entrapped in the polymer matrix and there are no chemical interactions between PTX and the copolymer.

3.3. The Specificity of Active Targeting Micelles in Cellular Levels *in Vitro*. *3.3.1. The Uptake in SSTR2-Expressing Tumor Cells.* Here, we chose two tumor cell lines with different SSTR2 expression levels in this study, human small cell lung cancer H446 cells (high SSTR2 expression) and human breast cancer MCF-7 cells (low SSTR2 expression).[34,52] The kinetic uptakes of PM-C6 and lanreotide-PM-C6 by these two cell lines at 37 °C are shown in Figure 2. It was clear that the cell endocytosis of active targeting micelles was much higher than that of passive targeting vesicles for both cell lines. In H446 cells, lanreotide-PM-C6 had a 1.81-, 1.83- and 2.24-fold uptake relative to that of PM-C6 (Figure 2A) after 1 h, 3 h and 6 h incubation at 37 °C, respectively, while the active targeting micelles demonstrated a 1.32-, 1.49-, 1.53-fold uptake relative to that of the passive group in MCF-7 cells at the same condition (Figure 2B). H446 cells internalized both micelle systems much faster and in greater amounts compared to MCF-7 cells, and the gap between active and passive group in H446 was also larger than that in the control cell line, very likely due to the difference in expression level of SSTR2 between these two cell lines.

As seen in Figure 2C, similar results were obtained in confocal microscopy images. Significantly increased intracellular fluorescence of C6 was observed with active targeting groups in

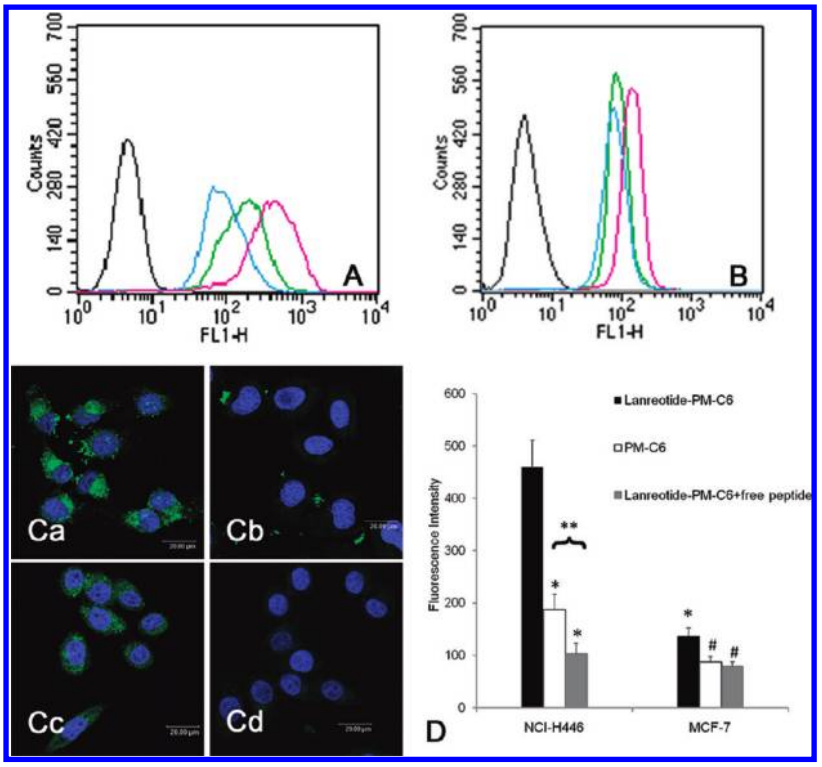

Figure 3. Competition experiments in cellular uptake by flow cytometry (A, B) and confocal microscopy images (C). In addition to the uptake test with active and passive groups, H446 cells (A, Cb) and MCF-7 cells (B, Cd) were pretreated with excess free lanreotide at 2.5 mg/mL, followed by incubation with lanreotide-PM-C6 (100 ng/mL C6 equivalent) for 6 h. H446 (Ca) and MCF-7 (Cc) were treated with active targeting micelles directly. In flow cytometric curves, red, green and blue represent lanreotide-PM-C6, PM-C6 and lanreotide-PM-C6 + free peptide, respectively. In confocal microscopy images, green and blue represent the C6 and Hoechst 33258, respectively. (D) Graphs of fluorescence intensity based on flow cytometric analysis. Each bar represents average fluorescence intensity ± SD (n = 3). *p < 0.01 vs lanreotide-PM-C6 in H446; #p < 0.05 vs lanreotide-PM-C6 in MCF-7; **p < 0.01. Enhanced cellular uptake by lanreotide modification was significantly blocked in the presence of free peptide.

both cell lines, whereas the fluorescence intensity in H446 cells was higher than that in MCF-7 cells, confirming the finding above.

3.3.2. Studies on the Uptake Mechanism. As indicated in Figure 3, in the presence of excess free lanreotide, fluorescence intensity of lanreotide-PM-C6 group in both cell lines decreased. Similar observations were noticed in both flow cytometry analysis (Figure 3A,B) and confocal microscopy study (Figure 3C). Figure 3D summarizes the quantitative results in flow cytometry analysis. First, the difference in cell uptake between the active and passive micelles in different cell lines was different. In H446, such difference was about 2.46 times, much larger than that in MCF-7 (about 1.57 times). Second, in the presence of excess free lanreotide, about 77.5% and 42.5% of cellular uptake was inhibited in H446 and MCF-7 cell lines, respectively. These values might basically indicate the ratio or the effect of receptor-mediated endocytosis in all cell uptake. Namely, specific and nonspecific uptake of lanreotide-PM-C6 in H446 cells was about 77.5% and 22.5%, respectively, while the values for the MCF-7 cell line were about 42.5% and 57.5%, respectively. In conclusion, the test demonstrated that most of the cell uptake of lanreotide-PM-C6 in H446 cells was due to the receptor-mediated endocytosis.

Overall, the above quantitative and qualitative results in cells consistently demonstrated that the specificity of micelles to tumor cells was highly dependent on the ligand modification as well as the expression level of SSTR2 in cells, and the intracellular endocytosis of lanreotide-PM-C6 in SSTR2-overexpressing cells was mostly receptor mediated.

3.4. The Targeting Effect of Lanreotide-Modified Micelles *in Vivo*. *3.4.1. In Vivo Distribution Studies by NIRF Imaging.* Previous photophysical experiments on carbocyanine fluorescent dye suggested that, at low occupancy (>1:100), the dye existed in a nonquenched state in the cores of PEG-b-PCL micelles and displayed high fluorescence quantum yields as free state.[53] Figure 4A shows the *in vivo* NIR fluorescence images of H446 tumor-bearing mice at different time after iv injection of free DiD, PM-DiD or lanreotide-PM-DiD.

First, it was found that different groups demonstrated different elimination rates. In the free DiD group, the signal elimination in body could be seen after first observation. The DiD signal intensity in the PM-DiD and lanreotide-PM-DiD groups was similar at 10 min, and then varied between different groups. The systemic fluorescence of DiD in the lanreotide-PM-DiD group was increasing gradually in the whole body until the end of test, while that in the PM-DiD group basically remained for about 10 h and increased partially at 24 h. This observation demonstrated that the active targeting group exhibited the slowest clearance.[54] In other words, this test showed the long circulation effect of both micelle systems.

Second, in the free DiD group, the fluorescent signal in the tumor was hardly detectable even from the first point, suggesting no specific distribution of free dye molecules in the tumor. However, in both micelle systems, the signals in

dx.doi.org/10.1021/mp200464x | *Mol. Pharmaceutics* 2012, 9, 1175−1188

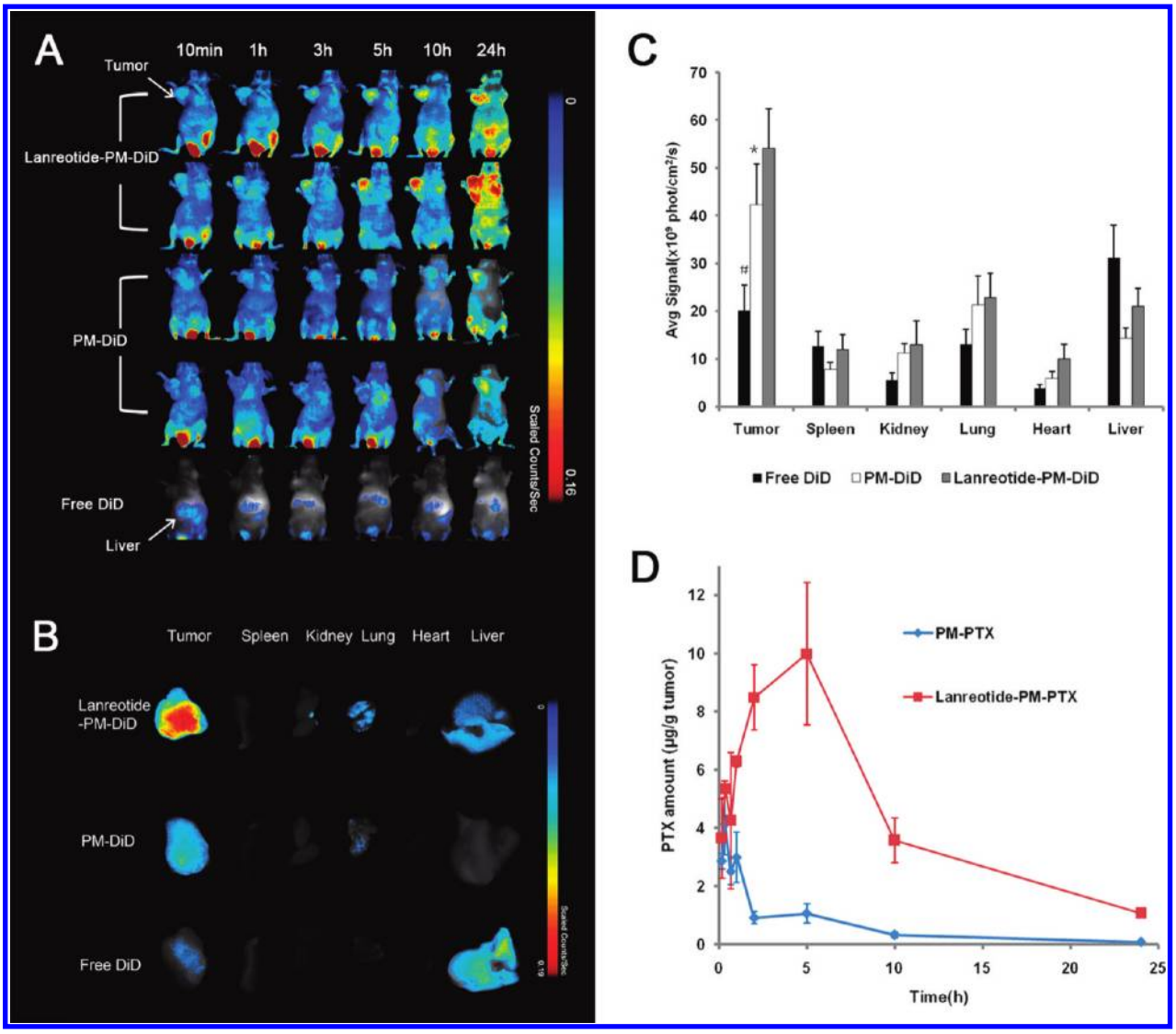

Figure 4. (A) *In vivo* NIR fluorescence imaging of H446 tumor-bearing mice at 0.17, 1, 3, 5, 10, and 24 h after iv injection of free DiD, PM-DiD or lanreotide-PM-DiD. (B) *Ex vivo* imaging of tumor and organs excised from H446 tumor-bearing mice at 24 h. (C) Analysis of fluorescence signal in tumor and organs from *ex vivo* imaging at 24 h. The mice were divided into four groups and injected with 5% glucose (data not shown), free DiD, PM-DiD and lanreotide-PM-DiD, respectively (DiD, λ_{ex} 644 nm, λ_{em} 663 nm). Data represent means ± SD (n = 3). $^{*}p < 0.05$, $^{\#}p < 0.01$ vs lanreotide-PM-DiD for fluorescence signal in tumor. (D) Accumulation of the PM-PTX and lanreotide-PM-PTX in the tumor tissues monitored by HPLC. Experiments were carried out using H446 tumor-bearing BALB/c nude mice (female, 5 weeks old, n = 6) when the tumor volume reached 300 mm^3. PM-PTX and lanreotide-PM-PTX were intravenously administered via lateral tail veins at a dose of 400 μg of PTX/mouse. Data represent mean ± SD (n = 6).

tumor increased during the test period of 0.17−24 h, possibly benefitting from the favorable EPR effect. Most importantly, the lanreotide-PM-DiD group showed a much stronger signal in the tumor site than that of the PM-DiD group at most time points. This provided solid evidence in the active targeting effect of lanreotide-modified micelles prepared.

Finally, we noticed that significant fluorescence in the free DiD group was found in liver from the first point, while in the other two groups the fluorescent signal in liver was rather weak compared to their intensity in the tumor. This was consistent with the previous observation on the favorable liver distribution of free DiR.[55] It was likely due to the lipophilic characteristics of carbocyanine dye (e.g., DiD, DiR, indocyanine green) which could be taken up exclusively by hepatic parenchymal cells and was secreted entirely into the bile.[56] Additionally, pegylated micelles might increase the accumulation of drug loaded in tumor and escape the capture of the reticuloendothelial system (RES) at least to some extent. By the way, it is possible that the distribution of free fluorescent dye in liver may be underestimated due to its decomposition or binding with proteins in liver, since its exposure here may be higher than micelles which release dye slowly. This may be the limitation of the fluorescence approach. Additionally, the higher body signal in active targeting micelles may be the result of its slow clearance,[54] possibly due to the high affinity of lanreotide-conjugated micelles to SSTRs. The SSTRs are the endogenous receptor distributing in the neuroendocrine system of the whole body, although overexpression was observed in the tumor cells in this system. As for the much brighter fluorescence in the site of the tail vein injection, we thought that it might be due to the local damage caused by the physical high pressure from the local injection.

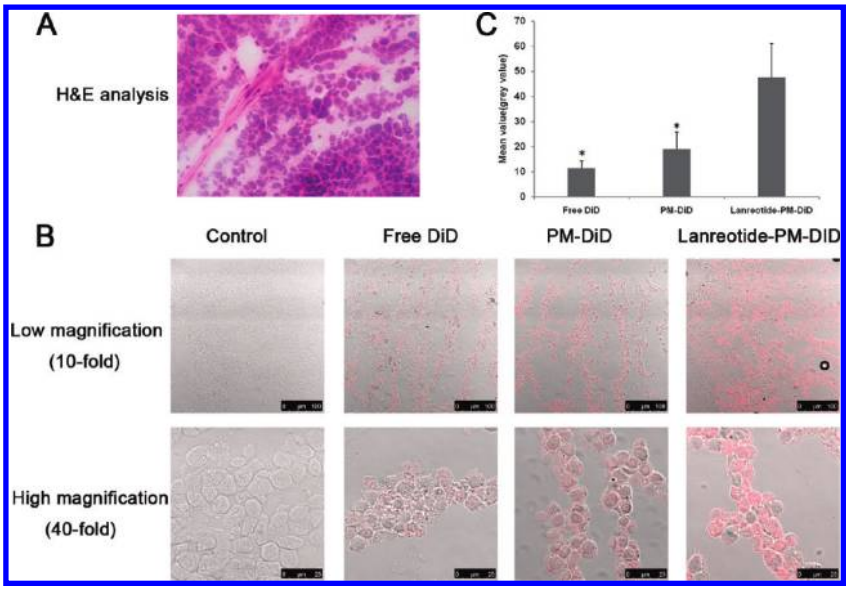

Figure 5. (A) Histological (H&E) analysis of tumor sample from frozen sections. (B) Confocal microscopy images of tumor frozen sections from H446 bearing nude mice 24 h after injection with 5% glucose, free DiD, PM-DiD or lanreotide-PM-DiD. The bright-field and fluorescence images were overlaid. The concentration of DiD was 100 μg/kg for all formulations. Red represents fluorescence of DiD. Magnification, ×10 or ×40. (C) Quantitative analysis of DiD fluorescence in tumor frozen sections. *p < 0.01 vs lanreotide-PM-DiD.

To confirm the *in vivo* fluorescence imaging, we further investigated the excised organs and tumor tissues in free DiD, PM-DiD and lanreotide-PM-DiD groups by *ex vivo* fluorescence imaging (Figure 4B), and their semiquantified data are shown in Figure 4C. The fluorescence signal intensity of *ex vivo* imaging is considered as a real reflection of the probes retained inside the organs because of lower or even no autofluorescence in the *ex vivo* images.[57] As shown in Figure 4B, there were almost no detectable DiD signals observed from kidney, spleen and heart for all the treatments, with very low values accordingly in Figure 4C. Again, compared to the other two groups, lanreotide-PM-DiD demonstrated the highest fluorescent density in the tumor, which was also much higher than that in other organs including liver and lung within the active targeting group. Although lower than that in the lanreotide-modified group, the fluorescent signal in the PM-DiD group mostly accumulated in the tumor with a little in the lung. In contrast, the fluorescence of free DiD was stronger in liver, much higher than its distribution in tumor. Together, it was clear that the lanreotide-PM-DiD exhibited the best targeting effect, followed by PM-DiD, while the free DiD showed no specificity to tumor tissue in biodistribution.

3.4.2. In Vivo Distribution Studies by HPLC. Figure 4D shows the drug accumulation in the tumor monitored by HPLC after the intravenous injection of each micelle system. The maximum drug level in tumor was 4.14 μg/g at 0.33 h for PM-PTX and 10.0 μg/g at 5 h for lanreotide-PM-PTX group, and these data represented 1.04% and 2.50% of injected dose/g of tumor tissue, respectively. The AUC_{0-24} of PM-PTX and lanreotide-PM-PTX was 14.2 ± 0.4 and 95.1 ± 4.1 h μg/g, respectively, which means a 6.70 times higher distribution in the active targeting group than that in the passive targeting group. These data suggest that lanreotide modified polymeric micelles possess the ability to deliver large amounts of PTX to the tumor site by passive targeting with a long-circulating carrier and the specific binding with H446 cells by lanreotide modification. Here, PTX exhibited faster elimination rate compared to DiD, revealing the difference between PTX and DiD. Due to the property of lipophilic carbocyanine dye, DiD retains its fluorescence in cells for several days.[58] It was reported previously that the signal of free DiD in mouse could be seen 24 h after a single tail vein injection.[59]

3.4.3. In Vivo Cellular Uptake Studies. The NIR fluorescence image above demonstrated the targeting effect of lanreotide-PM-DiD into tumor tissue, and we sought to understand this effect in tumor cells *in vivo*. H&E analysis in Figure 5A confirmed the tissue morphology and cell structure of a standard frozen section from the solid tumor tested.

Figure 5B shows overlay of bright-field and fluorescence images of tumor frozen sections from H446 bearing nude mice 24 h after different treatments. At low magnification (10-fold), confocal microscope indicated the location of DiD in cluster of tumor cells within tumor tissue, while at high magnification (40-fold), confocal pictures could clearly reveal the accumulation of DiD in tumor cells. It was found that the red fluorescence of DiD was mostly inside of tumor cells in the three test groups, so this study might be significant in terms of confirming the targeting of drug into the tumor cells. Obviously, the fluorescence of tumor cells in the lanreotide-PM-DiD treated group was much stronger, followed by that in the PM-DiD and free DiD groups in sequence, suggesting that lanreotide-PM-DiD could mostly enter into the SSTR-expressing tumor cells *in vivo*.

Additionally, the mean fluorescence value of ten different sections for each treatment was quantified (Figure 5C). The analysis showed high tumor cell uptake in the mice treated with lanreotide-PM-DiD (mean value of 49.27 ± 12.15), while the values for PM-DiD and free DiD were only 24.29 ± 5.52 and 14.55 ± 2.74, respectively. This result coincided with the result of NIRF imaging *in vivo* and the confocal image *in vitro*, and indicated that lanreotide-PM-DiD specifically targeted to H446 cancer cells and enhanced the accumulation in tumor cells.

The *in vivo* and *ex vivo* studies above demonstrated that the three formulations had different distribution and elimination characteristics. The drug in active targeting micelles eliminated the most slowly and distributed the most in tumor tissue and

tumor cells among the three groups. The results in this section were in agreement with that of cell tests *in vitro*.

3.5. Antitumor Activity of Lanreotide-Modified Micelles. *3.5.1. Antitumor Activity in Vitro.* The cytotoxicity of various PTX formulations against H446 cells is listed in Table 2. It was found that the IC_{50} value in active targeting micelles was much lower than that in passive targeting micelles. The free PTX was more cytotoxic than PM-PTX, likely due to the limited release of the drug from the micelles within a set period of time. However, this advantage of free PTX cannot be achieved *in vivo* because of its broad distribution in normal tissue and short circulation time. It is important to mention that this value of Taxol was the lowest among all formulations tested likely due to the toxicity of Cremophor EL and ethanol involved.[60] Finally, the blank micelles seemed biocompatible as shown in a previous study,[61] since there was no significant change in IC_{50} value after mixing with free PTX. We can thus conclude that conjugation of lanreotide to the surface of micelles plays a pivotal role in the cytotoxicity enhancement of PTX on the SSTR overexpressing tumor cells.

Table 2. Cytotoxicity of Various PTX Formulations against H446 Cells

PTX formulations	IC_{50}[a] (nM)
free PTX	27.7 ± 0.9[†]
free PTX + blank PM	29.2 ± 1.1[†]
Taxol	7.37 ± 0.67[*,†]
PM-PTX	74.5 ± 2.1*
lanreotide-PM-PTX	29.8 ± 0.7[†]

[a] $p < 0.01$ vs PM-PTX. [†] $p < 0.01$ vs free PTX.

3.5.2. Antitumor Activity in Vivo. Figure 6 and Table 3 display the suppression efficacy of various PTX formulations against nude mice bearing an H446 or MCF-7 tumor. As seen in Figure 6A, at the 17th day the tumor growth was significantly

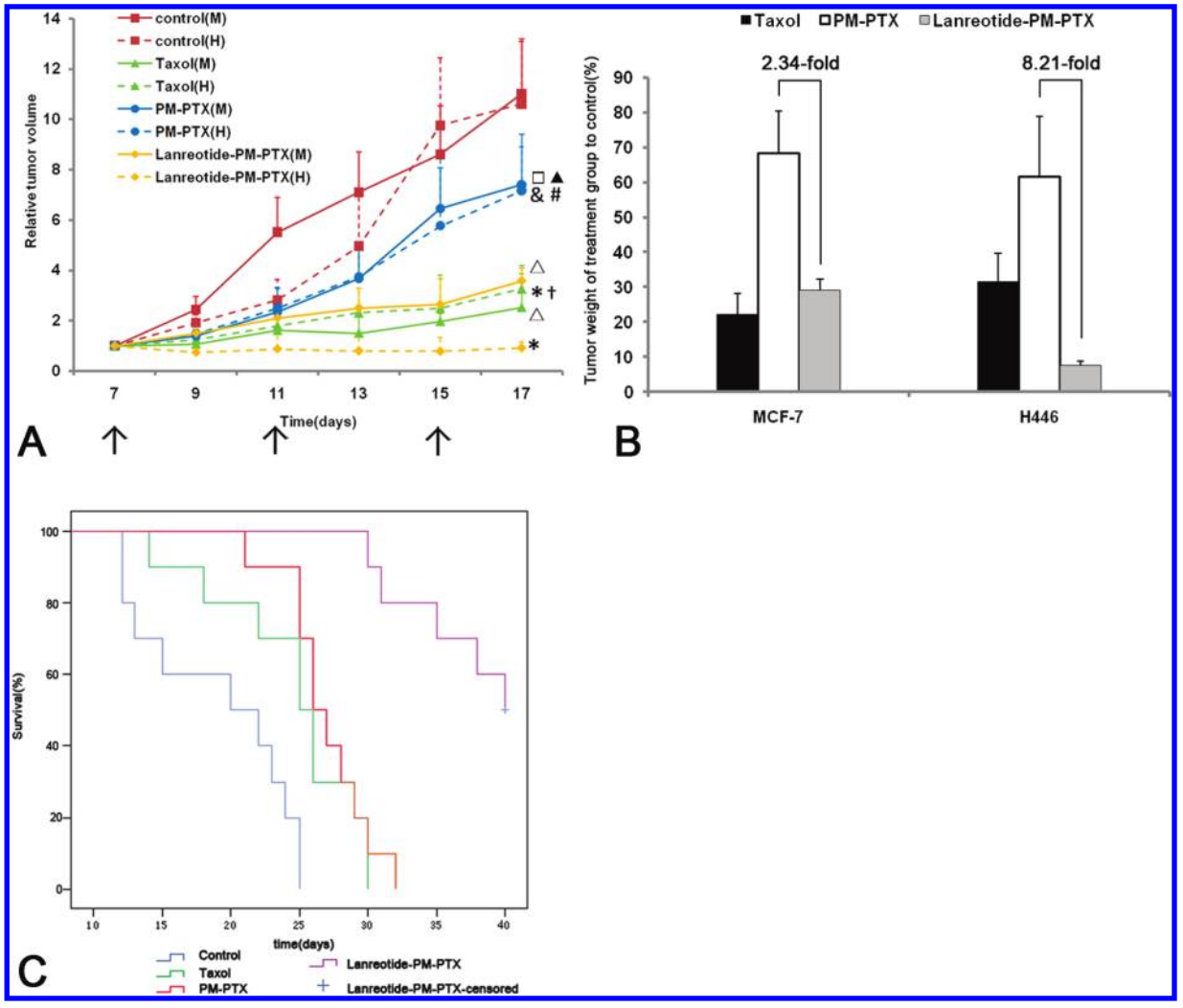

Figure 6. (A) Antitumor activity of 5% glucose, Taxol, PM-PTX and lanreotide-PM-PTX on nude mice bearing H446 (H) or MCF-7 (M) tumor. Relative tumor volume (RTV) was calculated according to the following formula: tumor volume on each day from 7th day to 17th day/tumor volume on the 7th day. □$p < 0.05$, $^{\Delta}p < 0.01$ vs control, ▲$p < 0.05$ vs lanreotide-PM-PTX in MCF-7 bearing mouse model; $^{\&}p < 0.05$, $^{*}p < 0.01$ vs control, $^{\dagger}p < 0.05$, $^{\#}p < 0.01$ vs lanreotide-PM-PTX in H446 tumor model. (B) The ratio of tumor weight of different PTX formulations to that of 5% glucose at the end of the test with nude mice bearing H446 or MCF-7 tumor. (C) Kaplan–Meier survival curve of nude mice bearing H446 tumors treated with various formulations. Treatment included 5% glucose (control), Taxol, PM-PTX and lanreotide-PM-PTX. Mice were given three iv injections of above formulations at a dose of 20 mg of PTX/kg at days 7, 11, and 15 after inoculation. The observation lasted for 40 days, and there were some mice in the lanreotide-PM-PTX group alive until the end of the experiment.

dx.doi.org/10.1021/mp200464x | *Mol. Pharmaceutics* 2012, 9, 1175–1188

Table 3. Antitumor Effects of Various PTX Formulations on H446 Tumor Bearing Nude Mice (n = 10)

	survival time (days)	median (days)	increased life span (%)	inhibn ratio of tumor vol (%)
control	19.1 ± 1.7	20		
Taxol	24.5 ± 1.7[a]	25	25.0	68.5
PM-PTX	26.9 ± 1.0[a,b]	26	30.0	38.3
lanreotide-PM-PTX	37.4 ± 1.2[a,c,d]	40	100	92.5

[a] $p < 0.01$ vs control . [b] $p > 0.05$ vs Taxol. [c] $p < 0.001$ vs Taxol. [d] $p < 0.001$ vs PM-PTX.

inhibited in all PTX groups compared to the 5% glucose group in two SSTR2 positive tumor bearing mouse models. Lanreotide-PM-PTX showed the strongest suppression on tumor growth among all PTX groups ($p < 0.05$ vs Taxol, $p < 0.01$ vs PM-PTX) in H446 tumor bearing mice. It was clear that the effect of PM-PTX on both cell lines was very similar, and there was a similar result for Taxol, while the effect of lanreotide-PM-PTX on high SSTR2 expressing tumor (H446) was significantly stronger than that on low SSTR2 expressing tumor (MCF-7), suggesting the involvement of receptor related.

Evaluated by the ratio of tumor weight to control (%) at the end of the test (Figure 6B), the lanreotide-PM-PTX group exhibited significantly better efficacy than PM-PTX in both tumor bearing mouse models. Importantly, such difference between lanreotide-PM-PTX and PM-PTX in H446 tumor bearing mice was about 8.21-fold, much larger than that in MCF-7 tumor bearing mice (2.34-fold). These results were consistent with the expression level of SSTR2 in different tumor cells and the *in vitro* comparison between these two cell lines. In general, this test demonstrated that the efficacy of lanreotide-PM-PTX *in vivo* was also related to the SSTR2 expression.

The antitumor effect of different treatments was also determined by the survival time and increased life span of H446 tumor-bearing mice as shown in Figure 6C and Table 3. Three PTX formulations were significantly more effective in prolonging mouse survival ($p < 0.01$) than 5% glucose. Mice treated with lanreotide-PM-PTX showed a significant increase in life span compared with mice receiving Taxol ($p < 0.001$) or PM-PTX ($p < 0.001$). Besides, although Taxol is more effective in the inhibition of tumor volume than PM-PTX, there was no significant difference in the survival time between these two groups.

Figure S3 in the Supporting Information shows the H&E staining of tumors from different treatment groups 17 days after H446 cell transplantation. The tumor tissues in each PTX group exhibited necrosis with different degrees. In mice treated with lanreotide-PM-PTX most tumor cells were severely damaged or destroyed. But, in the case of PM-PTX or Taxol, there was spotted or small focal necrosis. There was no necrosis observed in the control group. Besides, there was neither abscess formation nor purulent inflammation characterized by the absence of neutrophil and macrophage infiltration from the histological picture.

3.5.3. Tumor Apoptosis Analysis. In tumor tissues, cells undergoing apoptosis were subsequently examined using laser scanning confocal microscope after TUNEL staining. As shown in Figure 7, tumor tissues treated with lanreotide-PM-PTX induced the most apoptotic cells, while only a few scattered TUNEL-positive cells were visible after treatment with Taxol or PM-PTX. Glucose group had almost no effect on apoptosis as expected, resulting in negative TUNEL staining. We therefore concluded that lanreotide-PM-PTX increased the most apoptosis of cancer cells, thereby suppressing the tumor growth, and the results were in accordance with its antitumor activity above.

All studies on antitumor efficacy indicated that lanreotide-PM-PTX offered advantages in terms of enhancing tumor

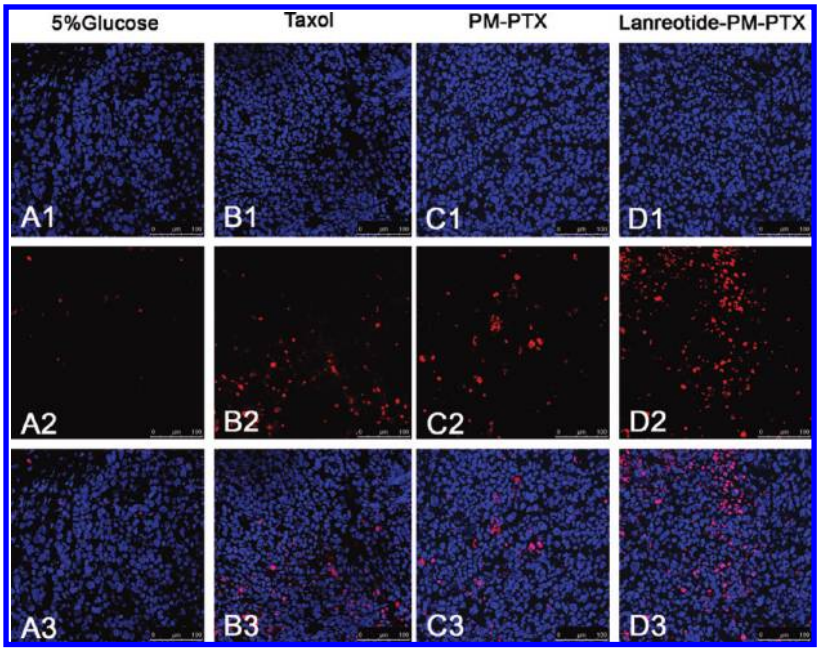

Figure 7. Confocal images of TUNEL assay for apoptotic cells in H446 tumor bearing in nude mice treated with (A1−3) 5% glucose; (B1−3) Taxol; (C1−3) PM-PTX and (D1−3) lanreotide-PM-PTX. DNA strand breaks were labeled with TMR red (red), and nuclei were stained with Hoechst 33258 (blue). Apoptotic cells exhibited pink color as a result of color merge of these two labels.

dx.doi.org/10.1021/mp200464x | *Mol. Pharmaceutics* 2012, 9, 1175−1188

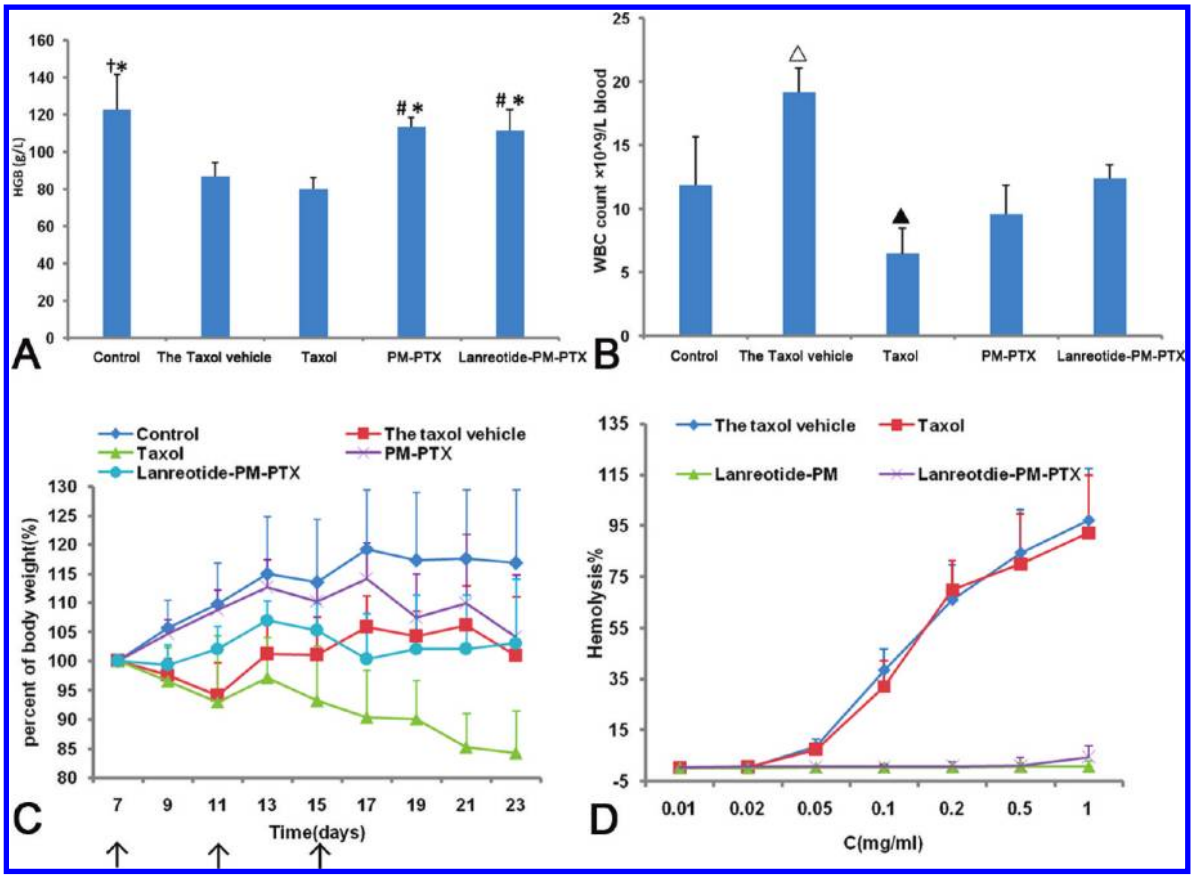

Figure 8. (A) Hemoglobin (HGB) and (B) white blood cell (WBC) counts from blood samples collected on day 22. Data represent the mean value ± SD of six mice per group. $^{*}p < 0.01$ vs mice treated with Taxol; $^{\#}p < 0.05$, $^{\dagger}p < 0.01$ vs mice treated with the corresponding Taxol vehicle. $^{\Delta}p < 0.01$ vs mice in other groups; ▲$p < 0.05$ vs mice treated with 5% glucose and lanreotide-PM-PTX. (C) The body weight change of H446-bearing nude mice after treatment with 5% glucose, Taxol vehicle, Taxol, PM-PTX or lanreotide-PM-PTX. (D) Hemolysis of red blood cell (RBC) as a function of concentration of Taxol, Taxol vehicle, lanreotide-PM-PTX or lanreotide-PM. Each point represents the mean value ± SD from three experiments.

inhibition, prolonging the life span of mice and increasing tumor cell apoptosis. This was also consistent with its increased drug distribution in tumor tissue and tumor cells.

3.6. Toxicity Studies. Figure 8 illustrates the HGB and WBC counts, body weight change and hemolysis data after different treatments. As shown in Figure 8A, mice receiving Taxol and the Taxol vehicle showed a marked and comparable decrease in HGB counts on day 22, likely due to hemolytic activity of Taxol vehicle. However, HGB counts were not significantly different in mice treated with PM-PTX, lanreotide-PM-PTX and 5% glucose. As shown in Figure 8B, Taxol exhibited a significant myelosuppression effect indicated by a marked decrease in WBC counts, whereas the Taxol vehicle brought about a dramatic WBC increase, probably because of its irritating and inflammatory effect;[62] and lanreotide-PM-PTX brought little effect on WBC compared to control group. Finally, all the treatment did not cause great changes in body weight of mice during test time except for Taxol with nearly 17% decrease on day 23 (Figure 8C).

As the concentration increased, hemolysis induced by Taxol and Taxol vehicle increased at a concentration from 0.02 to 1 mg/mL, while hemolytic activity of lanreotide-PM-PTX and lanreotide-PM was negligible even up to 1 mg/mL (Figure 8D). At a concentration of 1 mg/mL, hemolysis by Taxol and its vehicle reached 92.3% and 97.1%, respectively. The hemolysis by Taxol vehicle was very similar to that of Taxol, suggesting that hemolysis of Taxol was mostly resulted from its vehicle.

4. CONCLUSION

In this study, lanreotide was used as the targeting peptide to functionalize PEG-b-PCL micelles for specific targeting to SSTR2-positive tumor cells. The lanreotide modification on the micelles had little impact on the physicochemical properties of micelles in the test condition. In SSTR2-positive tumor cells, lanreotide modified PEG-b-PCL micelles demonstrated higher uptake over the passive targeting micelles via a somatostatin receptor mediated mechanism. Moreover, the active targeting micelles achieved preferential accumulation in tumor tissue and tumor cells. Furthermore, the treatment with lanreotide-PM-PTX resulted in an increased cytotoxicity in SSTR2-positive tumor cells *in vitro*, stronger tumor inhibition and increased life span in SSTR2-overexpressing tumor model in nude mice as well as enhanced tumor cell apoptosis *in vivo*. Better efficacy *in vivo* with H446 tumor model than that with MCF-7 tumor model further demonstrated the involvement of receptor-mediated targeting. Finally, the active targeting micelles exhibited less toxicity when compared to the control groups. There was a good correlation between *in vitro* and *in vivo* studies. It is therefore concluded that lanreotide may be used as a homing peptide and lanreotide-modified PEG-b-PCL micelles

developed here may serve as a promising delivery system in the treatment of SSTR2-overexpressing solid tumors.

■ ASSOCIATED CONTENT

Supporting Information

RP-HPLC assessment and ^{1}H NMR spectrum of lanreotide−PEG-b-PCL; XRD curves and FTIR spectra of PTX-loaded PEG-b-PCL micelles; histological (H&E) analysis of H446 tumors from different treatment groups. This material is available free of charge via the Internet at http://pubs.acs.org.

■ AUTHOR INFORMATION

Corresponding Author

*Department of Pharmaceutics, School of Pharmaceutical Sciences, Peking University, 38 Xueyuan Road, Haidian District, Beijing, 100191, China. E-mail: zqdodo@bjmu.edu.cn. Tel/fax: 86-10-82802791.

Notes

The authors declare no competing financial interest.

■ ACKNOWLEDGMENTS

This study was supported by National Science Foundation (No. 81130059) and Ministry of Science and Technology of China (No. 2009CB930300 and No. 2009ZX09310-001).

■ REFERENCES

(1) Savic, R.; Luo, L.; Eisenburg, A.; Maysinger, D. Micellar nanocontainers distribute to defined cytoplasmic organelles. *Science* **2003**, *300*, 615−618.

(2) Gaucher, G.; Dufresne, M. H.; Sant, V. P.; Kang, N.; Maysinger, D.; Leroux, J. C. Block copolymer micelles: preparation, characterization and application in drug delivery. *J. Controlled Release* **2005**, *109*, 169−188.

(3) Kataoka, K.; Harada, A.; Nagasaki, Y. Block copolymer micelles for drug delivery: design, characterization and biological significance. *Adv. Drug Delivery Rev.* **2001**, *47*, 113−131.

(4) Hubbell, J. A. Enhancing Drug Function. *Science* **2003**, *300* (5619), 595−596.

(5) Otsuk, H.; Nagasaki, Y.; Kataoka, K. PEGylated nanoparticles for biological and pharmaceutical applications. *Adv. Drug Delivery Rev.* **2003**, *55*, 403−419.

(6) Torchilin, V. P. Micellar Nanocarriers: Pharmaceutical Perspectives. *Pharm. Res.* **2007**, *24* (1), 1−16.

(7) Oerlemans, C.; Bult, W.; Bos, M.; Storm, G.; Nijsen, J. F. W.; Hennink, W. E. Polymeric Micelles in Anticancer Therapy: Targeting, Imaging and Triggered Release. *Pharm. Res.* **2010**, *27*, 2569−2589.

(8) Matsumura, Y. Poly (amino acid) micelle nanocarriers in preclinical and clinical studies. *Adv. Drug Delivery Rev.* **2008**, *60*, 899−914.

(9) Matsumura, Y.; Kataoka, K. Preclinical and clinical studies of anticancer agent-incorporating polymer micelles. *Cancer Sci.* **2009**, *100*, 572−579.

(10) Plummer, R.; Wilson, R. H.; Calvert, H.; Boddy, A. V.; Griffin, M.; Sludden, J.; et al. A Phase I clinical study of cisplatin-incorporated polymeric micelles (NC-6004) in patients with solid tumours. *Br. J. Cancer* **2011**, *104* (4), 593−598.

(11) Danson, S.; Ferry, D.; Alakhov, V.; Margison, J; Kerr, D.; Jowle, D.; et al. Phase I dose escalation and pharmacokinetic study of pluronic polymer-bound doxorubicin (SP1049C) in patients with advanced cancer. *Br. J. Cancer* **2004**, *90*, 2085−2091.

(12) Kim, T, Y.; Kim, D. W.; Chung, J. Y.; et al. Phase I and Pharmacokinetic Study of Genexol-PM, a Cremophor-Free, Polymeric Micelle-Formulated Paclitaxel, in Patients with Advanced Malignancies. *Clin. Cancer Res.* **2004**, *10*, 3708−3716.

(13) Mahmud, A.; Xiong, X. B.; Aliabadi, H. M.; Lavasanifar, A. Polymeric micelles for drug targeting. *J. Drug Targeting* **2007**, *15* (9), 553−584.

(14) Park, E. K.; Kim, S. Y.; Lee, S. B.; Lee, Y. M. Folate-conjugated methoxy poly(ethylene glycol)/poly(ε-caprolactone) amphiphilic block copolymeric micelles for tumor-targeted drug delivery. *J. Controlled Release* **2005**, *109*, 158−168.

(15) Wang, Y.; Yang, T.; Wang, X.; Dai, W.; Wang, J.; Zhang, X.; et al. Materializing sequential killing of tumor vasculature and tumor cells via targeted polymeric micelle system. *J. Controlled Release* **2011**, *149* (3), 299−306.

(16) Dharap, S. S.; Wang, Y.; Chandna, P.; Khandare, J. J.; Qiu, B.; Gunaseelan, S.; et al. Tumor-specific targeting of an anticancer drug delivery system by LHRH peptide. *Proc. Natl. Acad. Sci. U.S.A.* **2005**, *102* (36), 12962−12967.

(17) Lee, H.; Hu, M.; Reilly, R. M.; Allen, C. Apoptotic epidermal growth factor (EGF)-conjugated block copolymer micelles as a nanotechnology platform for targeted combination therapy. *Mol. Pharmaceutics* **2007**, *4* (5), 769−781.

(18) Reubi, J. C.; Kvols, L.; Krenning, E.; Lamberts, S. W. J. Distribution of somatostantin receptors in normal and tumor tissue. *Metabolism* **1990**, *39* (Suppl. 2), 78−81.

(19) Volante, M.; Rosas, R.; Allìa, E.; Granata, R.; Baragli, A.; Muccioli, G.; et al. Somatostatin, cortistatin and their receptors in tumours. *Mol. Cell. Endocrinol.* **2008**, *286*, 219−229.

(20) Olsen, J. O.; Pozderac, R. V.; Hinkle, G.; Hill, T.; O'Dorisio, T. M.; Schirmer, W. J.; et al. Somatostatin receptor imaging of neuroendocrine tumors with indium-111 pentetreotide (Octreoscan). *Semin. Nucl. Med.* **1995**, *25* (3), 251−261.

(21) Reubi, J. C. Peptide receptors as molecular targets for cancer diagnosis and therapy. *Endocr. Rev.* **2003**, *24*, 389−427.

(22) Siehler, S.; Seuwen, K.; Hoyer, D. [125I][Tyr3]octreotide labels human somatostatin sst2 and sst5 receptors. *Eur. J. Pharmacol.* **1998**, *348* (2−3), 311−320.

(23) Bodei, L.; Cremonesi, M.; Zoboli, S.; Grana, C.; Bartolomei, M.; Rocca, P.; et al. Receptor-mediated radionuclide therapy with 90Y-DOTATOC in association with amino acid infusion: a phase I study. *Eur. J. Nucl. Med. Mol. Imaging* **2003**, *30* (2), 207−216.

(24) Shen, H. C.; Hu, D. Y.; Du, J. J.; Wang, X. W.; Liu, Y. G.; Wang, Y. W.; et al. Paclitaxel−octreotide conjugates in tumor growth inhibition of A549 human non-small cell lung cancer xenografted into nude mice. *Eur. J. Pharmacol.* **2008**, *60* (1−3), 23−29.

(25) Moody, T. W.; Fuselier, J.; Coy, D. H.; Mantey, S.; Pradhan, T.; Nakagawa, T.; et al. Camptothecin-somatostatin conjugates inhibit the growth of small cell lung cancer cells. *Peptides* **2005**, *26* (9), 1560−1566.

(26) Smith-Jones, P. M.; Bischof, C.; Leimer, M.; Gludovacz, D.; Angelberger, P.; Pangerl, T.; et al. DOTA-Lanreotide: A Novel Somatostatin Analog for Tumor Diagnosis and Therapy. *Endocrinology* **1999**, *140*, 5136−5148.

(27) Virgolini, I.; Szilvasi, I.; Kurtaran, A.; Angelberger, P.; Raderer, M.; Havlik, E.; et al. Indium-111-DOTA-Lanreotide: Biodistribution, Safety and Radiation Absorbed Dose in Tumor Patients. *J. Nucl. Med.* **1998**, *39* (11), 1928−1936.

(28) Banerjee, S.; Das, T.; Chakraborty, S.; Samuel, G.; Korde, A.; Srivastava, S.; et al. ^{177}Lu-DOTA-lanreotide: A novel tracer as a targeted agent for tumor therapy. *Nucl. Med. Biol.* **2004**, *31*, 753−759.

(29) Patel, Y. C. Somatostatin and Its Receptor Family. *Front. Neuroendocrin.* **1999**, *20*, 157−198.

(30) Tomassetti, P.; Migliori, M.; Gullo, L. Slow-release lanreotide treatment in endocrine gastrointestinal tumors. *Am. J. Gastroenterol.* **1998**, *93* (9), 1468−1471.

(31) Dhanikula, A. B.; Panchagnula, R. Localized paclitaxel delivery. *Int. J. Pharm.* **1999**, *183*, 85−100.

(32) Wei, X. W.; Gong, C. Y.; Gou, M. L.; Fu, S. Z.; Guo, Q. F.; Shi, S.; et al. Biodegradable poly(ε-caprolactone)−poly(ethylene glycol) copolymers as drug delivery system. *Int. J. Pharm.* **2009**, *381*, 1−18.

(33) Zhou, S. B.; Deng, X. M.; Yang, H. Biodegradable poly(ε-caprolactone)−poly (ethylene glycol) block copolymers: character-

ization and their use as drug carriers for a controlled delivery system. *Biomaterials* **2003**, *24*, 3563−3570.
(34) Zhang, J. L.; Jin, W.; Wang, X. Q.; Wang, J. C.; Zhang, X.; Zhang, Q. A Novel Octreotide Modified Lipid Vesicle Improved the Anticancer Efficacy of Doxorubicin in Somatostatin Receptor 2 Positive Tumor Models. *Mol. Pharmaceutics* **2010**, *7* (4), 1159−1168.
(35) Wang, X.; Wang, Y. G.; Chen, X. M.; Wang, J. C.; Zhang, X.; Zhang, Q. NGR-modified micelles enhance their interaction with CD13-overexpressing tumor and endothelial cells. *J. Controlled Release* **2009**, *139* (1), 56−62.
(36) Xiong, M. P.; Yáñez, J. A.; Remsberg, C. M.; Ohgami, Y.; Kwon, G. S.; Davies, N. M.; et al. Formulation of a Geldanamycin Prodrug in mPEG-b-PCL Micelles Greatly Enhances Tolerability and Pharmacokinetics in Rats. *J. Controlled Release* **2008**, *129* (1), 33−40.
(37) Cho, Y. W.; Lee, J.; Lee, S. C.; Huh, K. M.; Park, K. Hydrotropic agents for study of in vitro paclitaxel release from polymeric micelles. *J. Controlled Release* **2004**, *97*, 249−257.
(38) Panyam, J.; Sahoo, S. K.; Prabha, S.; Bargar, T.; Labhasetwar, V. Fluorescence and electron microscopy probes for cellular and tissue uptake of poly(D,L-lactide-co-glycolide) nanoparticles. *Int. J. Pharm.* **2003**, *262*, 1−11.
(39) Skehan, P.; Storeng, R.; Scudiero, D.; Monks, A.; McMahon, J.; Vistica, D.; et al. New Colorimetric Cytotoxicity Assay for Anticancer-Drug Screening. *J. Natl. Cancer Inst.* **1990**, *82* (13), 1107−1112.
(40) Agmon, A.; Yan, L. T.; Jones, E. G.; O'Dowd, D. K. Topological precision in the thalamic projection to neonatal mouse barrel cortex. *J. Neurosci.* **1995**, *15*, 549−561.
(41) Tian, T.; Wang, Y. Y.; Wang, H. T.; Zhu, Z. Q.; Xiao, Z. D. Visualizing of the Cellular Uptake and Intracellular Trafficking of Exosomes by Live-Cell Microscopy. *J. Cell. Biochem.* **2010**, *111*, 488−496.
(42) Mckenna, J.; Prusky, G. T.; Whishaw, I. Q. Cervical Motoneuron Topography Reflects the Proximodistal Organization of Muscles and Movements of the Rat Forelimb: A Retrograde Carbocyanine Dye Analysis. *J. Comp. Neurol.* **2000**, *419*, 286−296.
(43) Bilensoya, E.; Gürkaynak, O.; Doğan, A. L.; Hıncal, A. A. Safety and efficacy of amphiphilic β-cyclodextrin nanoparticles for paclitaxel delivery. *Int. J. Pharm.* **2008**, *347* (1−2), 163−170.
(44) Lee, J.; Lee, S. C.; Acharya, G.; Chang, C.; Park, K. Hydrotropic solubilization of paclitaxel: Analysis of chemical structures for hydrotropic property. *Pharm. Res.* **2003**, *20* (7), 1022−1030.
(45) Letchford, K.; Liggins, R.; Wasan, K. M.; Burt, H. In vitro human plasma distribution of nanoparticulate paclitaxel is dependent on the physicochemical properties of poly(ethylene glycol)-block-poly(caprolactone) nanoparticles. *Eur. J. Pharm. Biopharm.* **2009**, *71*, 196−206.
(46) Gao, H. J.; Shi, W. D.; Freund, L. B. Mechanics of receptor-mediated endocytosis. *Proc. Natl. Acad. Sci. U.S.A.* **2005**, *102* (27), 9469−9474.
(47) Riezman, H.; Woodman, P. G.; van Meer, G.; Marsh, M. Molecular mechanisms of endocytosis. *Cell* **1997**, *91* (6), 731−738.
(48) Yamamoto, Y.; Nagasaki, Y.; Kato, Y.; Sugiyama, Y.; Kataoka, K. Long-circulating poly(ethylene glycol)−poly(D,L-lactide) block co-polymer micelles with modulated surface charge. *J. Controlled Release* **2001**, *77*, 27−38.
(49) Beck-Broichsitter, M.; Thieme, M.; Nguyen, J.; Schmehl, T.; Gessler, T.; Seeger, W.; et al. Novel 'Nano in Nano' Composites for Sustained Drug Delivery: Biodegradable Nanoparticles Encapsulated into Nanofiber Non-Wovens. *Macromol. Biosci.* **2010**, *10* (12), 1527−1535.
(50) Shen, J.; Zhan, C. Y.; Xie, C.; Meng, Q. G.; Gu, B.; Li, C.; et al. Poly(ethylene glycol)-block-poly(D,L-lactide acid) micelles anchored with angiopep-2 for brain-targeting delivery. *J. Drug Targeting* **2011**, *19* (3), 197−203.
(51) Mei, H.; Shi, W.; Pang, Z. Q.; Wang, H. F.; Lu, W. Y.; Jiang, X. G.; et al. EGFP-EGF1 protein-conjugated PEG-PLA nanoparticles for tissue factor targeted drug delivery. *Biomaterials* **2010**, *31*, 5619−5626.
(52) Watt, H. L.; Kumar, U. Colocalization of somatostatin receptors and epidermal growth factor receptors in breast cancer cells. *Cancer Cell Int.* **2006**, *6*, 5−23.
(53) Cho, H.; Indig, G. L.; Weichert, J.; Shin, H. C.; Kwon, G. S. In Vivo Cancer Imaging by Poly(ethylene glycol)-b-poly(ε-caprolactone) Micelles Containing a Near-infrared Probe. *Nanomedicine* **2012**, *8* (2), 228−236.
(54) Su, Z. G.; Niu, J. X.; Xiao, Y. Y.; Ping, Q. N.; Sun, M. J.; Huang, A. W.; et al. Effect of Octreotide-Polyethylene Glycol(100) Monostearate Modification on the Pharmacokinetics and Cellular Uptake of Nanostructured Lipid Carrier Loaded with Hydroxycamptothecine. *Mol. Pharmaceutics* **2011**, *8* (5), 1641−1651.
(55) Guo, L. R.; Fan, L.; Pang, Z. Q.; Ren, J. F.; Ren, Y. L.; Li, J. W.; et al. TRAIL and doxorubicin combination enhances anti-glioblastoma effect based on passive tumor targeting of liposomes. *J. Controlled Release* **2011**, *154* (1), 93−102.
(56) Desmettre, T.; Devoisselle, J. M.; Mordon, S. Fluorescence Properties and Metabolic Features of Indocyanine Green (ICG) as Related to Angiography. *Surv. Ophthalmol.* **2000**, *45* (1), 15−27.
(57) Gao, J. H.; Chen, K.; Xie, R. G.; Xie, J.; Yan, Y. J.; Cheng, Z.; et al. In vivo Tumor-targeted fluorescence imaging using near-infrared non-cadmium quantum dots. *Bioconjugate Chem.* **2010**, *21*, 604−609.
(58) Parish, C. R. Fluorescent dyes for lymphocyte migration and proliferation studies. *Immunol. Cell Biol.* **1999**, *77*, 499−508.
(59) Xiao, K.; Luo, J.; Fowler, W. L.; Li, Y.; Lee, J. S.; Xing, L.; et al. A self-assembling nanoparticle for paclitaxel delivery in ovarian cancer. *Biomaterials* **2009**, *30* (30), 6006−6016.
(60) Soga, O.; van Nostrum, C. F.; Fens, M.; Rijcken, C. J. F.; Schiffelers, R. M.; Storm, G.; et al. Thermosensitive and biodegradable polymeric micelles for paclitaxel delivery. *J. Controlled Release* **2005**, *103*, 341−353.
(61) Kim, S. Y.; Lee, Y. M.; Baik, D. J.; Kang, J. S. Toxic characteristics of methoxy poly(ethylene glycol)/poly(ε-caprolactone) nanospheres: in vitro and in vivo studies in the normal mice. *Biomaterials* **2003**, *24*, 55−63.
(62) Banzato, A.; Bobisse, S.; Rondina, M.; Renier, D.; Bettella, F.; Esposito, G.; et al. A Paclitaxel-Hyaluronan Bioconjugate Targeting Ovarian Cancer Affords a Potent In vivo Therapeutic Activity. *Clin. Cancer Res.* **2008**, *14*, 3598−3606.